Chemical Engineering Journal 356 (2019) 178–189

Contents lists available at ScienceDirect

Chemical Engineering Journal

journal homepage: www.elsevier.com/locate/cej

Persulfate non-radical activation by nano-CuO for efficient removal of chlorinated organic compounds: Reduced graphene oxide-assisted and CuO (0 0 1) facet-dependent

Xiaodong Du[a], Yongqing Zhang[a,b,c,*], Fan Si[a], Chenhui Yao[a], Meimei Du[a], Imtyaz Hussain[d], Hyunook Kim[e], Shaobin Huang[a], Zhang Lin[a], Waseem Hayat[a]

[a] School of Environment and Energy, Guangdong Provincial Key Laboratory of Atmospheric Environment and Pollution Control, South China University of Technology, Guangzhou 510006, China
[b] The Key Lab of Pollution Control and Ecosystem Restoration in Industry Clusters, Ministry of Education, Guangzhou 510006, China
[c] State Key Laboratory of Pulp and Paper Engineering, South China University of Technology, Guangzhou 510640, China
[d] School of Environment, Jinan University, Guangzhou 510632, China
[e] Department of Environment Engineering, University of Seoul, Seoul 130-743, South Korea

HIGHLIGHTS

- Reduced graphene oxide enhanced persulfate activation on CuO surface by Cu–O–C bond.
- (0 0 1) facet-dependent persulfate non-radical activation by CuO was found.
- This non-radical system showed selective removal for chlorinated organic pollutants.

GRAPHICAL ABSTRACT

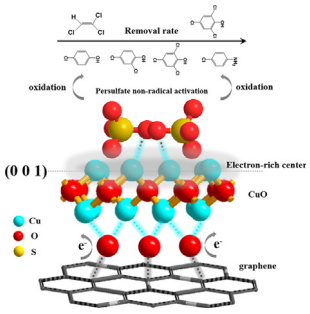

ARTICLE INFO

Keywords:
Persulfate
CuO
Non-radical activation
Selective removal
Crystal facet effect

ABSTRACT

Non-radical activation of persulfate by CuO to degrade chlorinated organic pollutants has been studied. Currently, reduced graphene oxide modified spindle-like CuO (CuO/rGO, no preferential exposed crystal facet) and CuO with preferential exposed crystal facet (0 0 1) (sheet-like CuO) has been prepared to improve the performance of persulfate activation. Results showed that CuO/rGO-persulfate system and sheet-like CuO-persulfate system exhibited much better 2,4,6-trichlorophenol (TCP) removal rate than spindle-like CuO-persulfate system. The formation of Cu–O–C bond between CuO and rGO enhanced the persulfate activation by CuO. On the other hand, CuO showed crystal facet effect on persulfate activation, and the crystal facet (0 0 1) of CuO (all exposed atoms were Cu) were proved to be efficient for persulfate non-radical activation, revealing that Cu atom on surface was active site for persulfate activation. Furthermore, the pollutants selective removal by CuO/rGO-persulfate system has been found. 4-chloroaniline was most easily degraded, followed by 2,4,6-trichlorophenol, 2,4-dichlorophenol and 4-chlorophenol, under acidic, neutral and weak basic condition (pH 3–9). What's more, pollutants with benzene ring was more reactive than that with double bond of carbon in the system.

* Corresponding author at: School of Environment and Energy, Guangdong Provincial Key Laboratory of Atmospheric Environment and Pollution Control, South China University of Technology, Guangzhou 510006, China.
E-mail address: zhangyq@scut.edu.cn (Y. Zhang).

https://doi.org/10.1016/j.cej.2018.08.216
Received 3 April 2018; Received in revised form 28 August 2018; Accepted 30 August 2018
Available online 31 August 2018
1385-8947/

1. Introduction

Efficient catalysts are critical for persulfate (PS) based advanced oxidation technologies (AOTs) to remove organic pollutants. Since more and more PS-based AOTs are implemented in water treatment and environmental remediation [1–4], the heterogeneous catalysts draw researchers' attention due to the lower cost and higher applicability [5]. Traditionally, heat, base, UV-light, transition metal ions drive the persulfate activation to generate sulfate radical ($E^0(SO_4^{-}\cdot/SO_4^{2-})$ = 2.5–3.1 V vs. NHE), the counterpart of omnipotent hydroxyl radical ($E^0(\cdot OH/OH^-)$ = 1.8–2.7 V vs. NHE), to oxidize organic pollutants [6]; as studies move on, these homogeneous catalysis methods keep on developing, including the development of electro-catalysis [7] and sonication activation of persulfate [8]. Interestingly, more and more newly developed heterogeneous catalysts based persulfate activation methods spring up, including iron-based [9–11], transition metal oxide-based [12–16], naturally occurring mineral-based [17–19] and carbon-based technologies [20–26], for the advantages of less energy or chemicals input and less second pollution output compared with traditional technologies. Among the numerous methods, iron-based heterogeneous material is the pioneer with high persulfate activation efficiency [9]. Minerals such as pyrite, pyrrhotite, clay and other naturally occurring species have successfully activated persulfate to degrade organic pollutants [17–19], giving the powerful support for in situ chemical oxidation (ISCO). Being free of heavy metals, carbon based materials are green catalysts. Carbons with different morphologies like nanotubes [24], activated carbon [23], diamond crystal [27], biochar [14], hierarchically porous carbon [22] and graphene [21] are capable of activating persulfate. Without exception, the catalysts mentioned above activate persulfate to generate sulfate radicals, a strong oxidative species, to oxidize refractory organic pollutants.

Recently, a mild persulfate activation process has been proposed—non-radical activation mechanism, the activated persulfate directly reacts with target pollutants without prior peroxy bond split to generate sulfate radical [27–31]. The newly published paper summarizes that transition metals initiate one-electron reduction of persulfate to sulfate radical, whereas some carbonaceous nanomaterial mediate the electron transfer from organic pollutants to persulfate, namely non-radical mechanism [27,30,31]. Interestingly, different from other transition metal oxides or ions, the copper oxide also mediates the non-radical mechanism. Zhang et al. [28] and Du et al. [29] found that the persulfate solution remained stable after the addition of copper oxide, while the introduction of organic pollutants resulted in the persulfate decomposition.

This phenomenon indicates the persulfate non-radical activation by CuO; if the process follows the sulfate radical activation mechanism, persulfate would be consumed continuously because of persistent sulfate radical generation and radical propagation reaction. Scavenger study, Attenuated Total Reflection Fourier Transform Infrared spectrum (ATR-FTIR), Confocal Raman spectrum and Electron Paramagnetic Resonance spectrum further demonstrate the non-radical activation mechanism [28,29]. The mechanism shows the following remarkable advantages in organic pollutants oxidation: (1) halide organic intermediates generation decreases due to the inhibition of halide radical production resulted from reaction between halide ion and sulfate radical or else [32–34], (2) self-quenching by radical propagation reaction is avoided, the oxidation capacity of persulfate is fully used, (3) the relatively mild activated persulfate oxidizes target organic pollutants selectively but hydroxyl radical and sulfate radical attack most of the organic pollutants. Therefore the copper oxide is a preferential choice as catalyst to activate persulfate in our study.

To further enhance the persulfate activation efficiency, the reduced graphene oxide (rGO) is selected as a supportive material for copper oxide. It has been reported that the bond of Cu–O–C formed between CuO and π bond-containing material would cause the electron-rich center at CuO to activate H_2O_2 [35]. It is supposed that the interaction between CuO center and persulfate would be enhanced by electron relocation. Hence the CuO/rGO composite has been prepared in this work: (1) To fully use the electron-rich center to increase persulfate activation efficiency, and (2) To anchor copper oxide on two-dimensional or three-dimensional graphene to get CuO with nano scale size and higher dispersity. On the other hand, it is reported that exposed crystal facet of CuO plays an important role in catalysis [36], hence it is a good point of view to enhance persulfate activation efficiency by controlling the exposed facet or crystal growth direction of CuO. Yet various CuO with different morphology have been prepared by different methods as reported [37]. In this work, persulfate activation by CuO with different morphology was also studied, to find out the relationship between exposed facet and persulfate activation efficiency by analyzing exposed facet of different morphology CuO.

Environmental pollution has been one of the global issues. There are more than 4 billion people facing severe water scarcity [38]. Water contamination intensifies the tendency of water scarcity and threatens the public health. Refractory chloride aromatic compounds are one of the persistent and toxic pollutants in water, listed as priority pollutants in water by China and United States. Chlorophenols, one of chloride aromatic compounds, are major group of pollutants of environmental concern because of their toxicity and widespread uses [39], they are recalcitrant to biodegradation and are therefore persistent in the environment [40]. Chlorophenols usually exist in fungicide, glue preservative, insecticide, bactericide, defoliant, herbicide, and anti-mildew agent for textiles; they also could be transformed from biodegradation of herbicides and pesticides, or combustion of organic matters. Therefore chlorophenols are frequently found in wastewater, sludge products, surface waters, and groundwater [40]. The principal point source of water pollution by chlorophenols is industrial waste discharge and leaching of chlorophenols from landfills [41]; the primary nonpoint source pollution of chlorophenols comes from the application of pesticides that are made from chlorophenols and the chlorination of wastewater containing phenol [42]. 2,4,6-Trichlorophenol (2,4,6-TCP), one of the toxic chlorophenols, it is reasonably anticipated to be a human carcinogen [39,43], and frequently detected in China surface water [44]. Therefore the 2,4,6-TCP is selected as the target pollutant, giving the perspective to evaluate the mechanism of CuO-persulfate-pollutant interaction.

2. Experimental

2.1. Chemicals and materials

All chemicals used in experiments were analysis reagent (AR) and HPLC reagent (HPLC)

Persulfate (AR) was purchased from Chengdu Kelong Chemical Reagent Factory (Chengdu, China). 2,4,6-Trichlorophenol (TCP, AR), 2,4-dichlorophenol (DCP, AR), 4-chlorophenol (CP, AR), trichloroethylene (TCE, AR), 5, 5-Dimethyl-1-pyrroline N-oxide (DMPO, AR), dichloromethane (HPLC) and methanol (HPLC) were purchased from Shanghai Aladdin Company (Shanghai, China). 4-Chloroaniline (PCA, AR) was purchased from Sigma-Aldrich Chemical Company (Shanghai, China). Ethanol (AR), H_2SO_4 (AR), H_3PO_4 (AR) and $Cu(NO_3)_2{\cdot}3H_2O$ (AR) were purchased from Guangzhou Chemical Reagent Factory (Guangzhou, China). Graphite powder (AR), $NaHCO_3$ (AR), Na_2CO_3 (AR) and NaCl (AR) were purchased from Tianjin Damao Chemical Reagent Factory (Tianjin, China). H_2O_2 (AR) and NaOH (AR) were purchased from Sinopharm chemical reagent Co. Ltd. Potassium iodide (AR) was purchased from Shanghai Titan Company (Shanghai, China). $CuSO_4{\cdot}5H_2O$ (AR) was purchased from Tianjin Fuchen Chemical Reagent Factory (Tianjin, China). Formic acid (HPLC) was purchased Xiya reagent Company (Shandong, China).

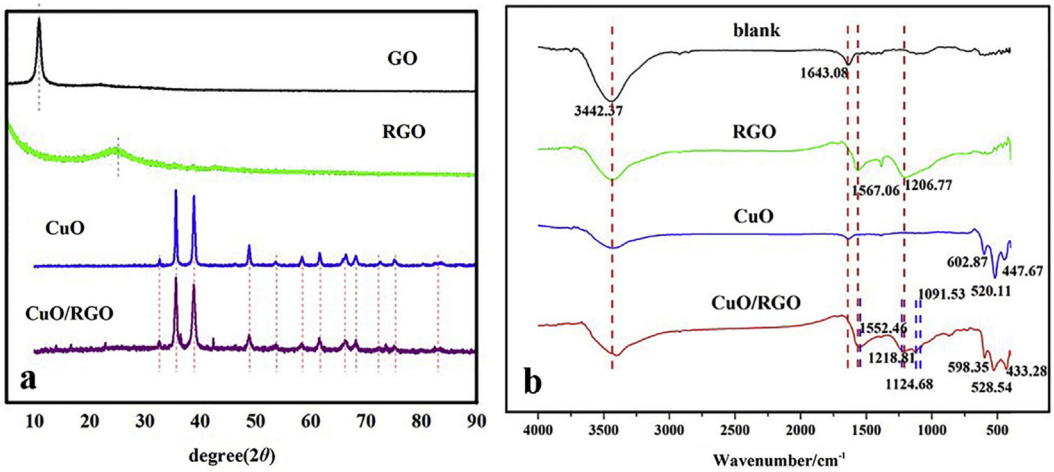

Fig. 1. (a) XRD patterns of GO, rGO, CuO and CuO/rGO$^{2:1}$; (b) FTIR spectrum of rGO, CuO and CuO/rGO$^{2:1}$.

2.2. Experimental procedures

2.2.1. Material synthesis

Graphene oxide was synthesized by improved hummer's method [45], reduced graphene oxide (rGO) and CuO/rGO composite were prepared by hydrothermal method. Spindle-like and sheet-like CuO [37] were prepared by hydrothermal methods, sphere-like CuO was prepared by calcination method. All preparation details were described in Supplementary material (Text 1).

2.2.2. Sample preparation

2.2.2.1. All experiments were in batch mode. Initially, 2 mmol·L^{-1} TCP (DCP, CP, PCA) stock solution and 50 mmol·L^{-1} PS stock solution were prepared using deionized water. Before beginning the reaction, initial aqueous solution was prepared by diluting 5 mL pollutant stock solution with 90 mL deionized water in a 250 mL flask. Then the flask was fixed in a shaker, being shaken at the speed of 125 rpm at 25 °C for 10 min. An aliquot of the mixture (0.5 mL) was sampled and filtered through 0.45 μm filters, followed by being injected into 1.5 mL vials with 0.5 mL preloaded 20 mmol·L^{-1} sodium thiosulfate solution. These samples were prepared for analysis of the initial pollutant concentration by HPLC. To start the reaction, 0.01 g material was put into a flask, followed by addition of 5 mL PS stock solution. Samples were taken regularly by following the procedure described above. Preparation procedures of sampling for GC–MS, Ion Chromatography, TOC and Electron Paramagnetic Resonance were described in Supplementary material (Text 2).

2.3. Analysis methods

High performance liquid chromatography (HPLC, Shimadzu LC-20A, Diode Array Detector, Kyoto, Japan) was used to determine the concentrations of 2,4,6-Trichlorophenol (TCP), 2,4-Dichlorophenol (DCP), 4-Chlorophenol (CP) and 4-Chloroaniline (PCA). Substance separation was achieved by a C18 column purchased from Agilent (250 mm × 4.6 mm, 5 μm; Santa Clara, California, USA), with methanol and 0.1% formic acid (90/10, 1 mL/min for 2, 4, 6-Trichlorophenol; 90/10, 0.8 mL/min for 2,4-Dichlorophenol; 70/30, 0.6 mL/min for 4-Chlorophenol and 4-Chloroaniline) as mobile phase. The detection channels for 2,4,6-Trichlorophenol, 2,4-Dichlorophenol, 4-Chlorophenol and 4-Chloroaniline were 290 nm, 284 nm, 284 nm, and 244 nm, respectively.

Trichloroethylene and intermediates of 2,4,6-Trichlorophenol were tested by Gas Chromatograph-Mass Spectrometer (GCMS, Agilent 7890A-5875C). Persulfate was determined by Iodine colorimetric spectrophotometric method improved by Liang [46]. Chloride ion was detected by Ion Chromatography (Dionex, ICS 1000, AS 14 column). TOC removal was tested by Elementar vario TOC. Radicals in solution were identified by Electron Paramagnetic Resonance (Bruker A300). Atomic Absorption Spectroscopy (AA-6300C, Shimadzu, Kyoto, Japan) has been used for determination of Cu^{2+} leaching from material. All test conditions and parameters were stated in Supplementary material (Text 3).

X-ray diffraction (XRD, Empyrean) was applied to confirm the successful preparation of CuO and CuO/rGO. Scanning electron microscope (SEM; Hitachi SU8010, Japan) was applied to observe the morphology of composites. Transmission electron microscope (TEM; Tecnai G2 F20 S-TWIN, 200KV, Japan) was applied to observe the morphology, structure, and exposed crystal facet of composites. Fourier transform infrared spectroscopy (FTIR; Nicolet 6700, USA) was applied to find the evidence of bond formation. Thermogravimetric analysis (TGA; NETZSCH STA 449 C, Germany) was applied to determine the mass ratio of different components of the composite; the temperature was increased from 30 °C to 800 °C at rate of 10 °C/min. Brunauer-Emmett-Teller (BET) specific surface area was characterized by Autosorb iQ Station 1 (USA), to fully describe the interior structure properties of the composite.

3. Results and discussion

3.1. Characterization

XRD patterns of hydrothermally synthesized CuO, rGO and CuO/rGO$^{2:1}$ were compared in Fig. 1a. As shown in the figure, all the materials were successfully prepared. CuO pattern matched well with PDF card (#89-5899, CuO). The rGO pattern was the same as the reported typical pattern of 3-dimension reduced graphene oxide prepared at higher temperature by hydrothermal reduction [47]. CuO/rGO$^{2:1}$ pattern included all characteristic peaks of CuO; the disappearance of rGO peak bump at 25° (2θ) might be ascribed to the destruction of rGO oxygen group or structure periods by CuO growth. The XRD patterns of CuO/rGO$^{10:1}$, CuO/rGO$^{4:1}$, CuO/rGO$^{1:1}$, CuO/rGO$^{1:2}$, CuO/rGO$^{1:4}$, CuO/rGO$^{1:10}$, CuO/rGO$^{1:20}$ are listed in Supplementary material (Fig. S1).

The SEM and TEM pictures of CuO/rGO$^{2:1}$ showed that CuO had well-grown on rGO (Fig. 2). The small rock-like CuO pieces aggregated to form spindle-like or unshaped spindle-like CuO bulks. The selected area electron diffraction (SAED) of TEM verified the polycrystalline structure of CuO. The size of CuO was from nano-meters to micro-meters. The rGO showed a 3-dementional structure with CuO on the surface or between sheets. TEM pictures displayed a more clear perspective of "rocks on ship" relationship between CuO and rGO. The SEM and

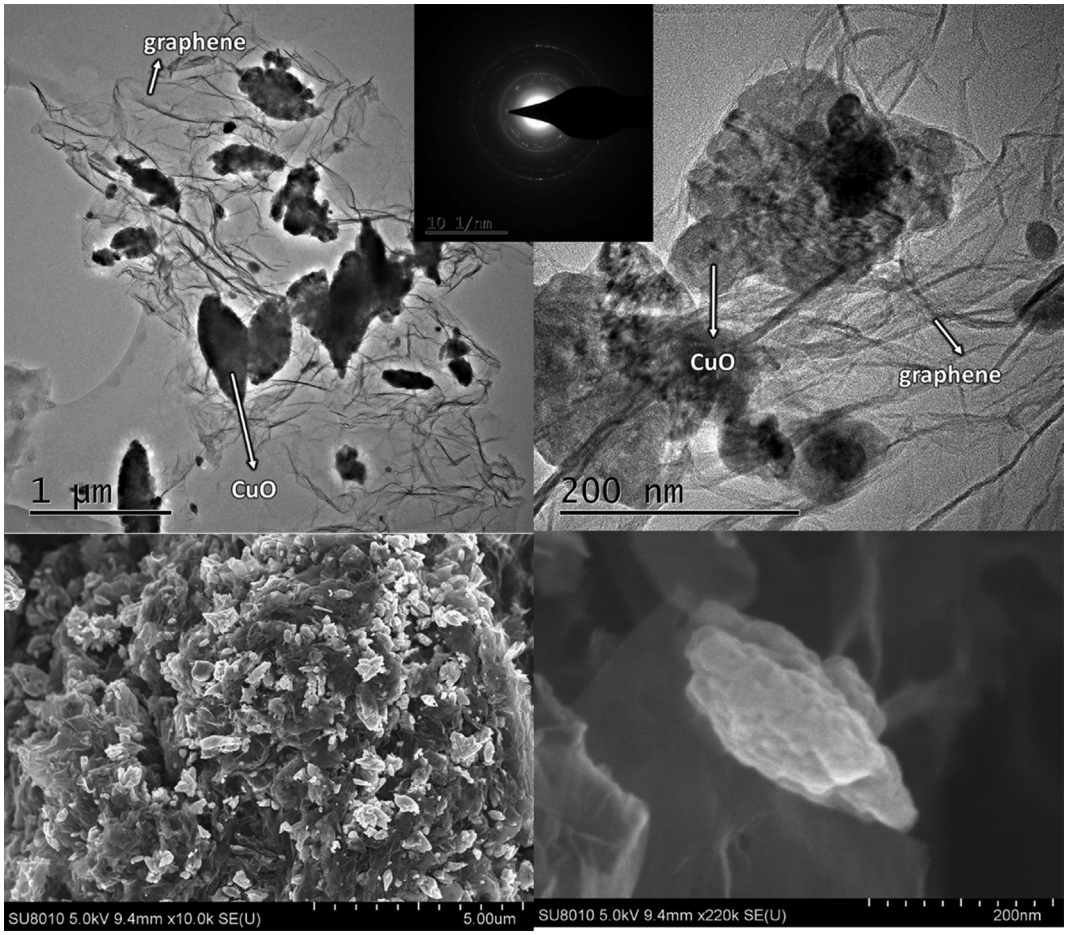

Fig. 2. SEM and TEM images of $CuO/rGO^{2:1}$.

TEM images of sheet-like and sphere-like CuO were listed in Supplementary material (Figs. S2–S6). The SEM of $CuO/rGO^{1:1}$, $CuO/rGO^{4:1}$, $CuO/rGO^{10:1}$, CuO and rGO are listed in Supplementary material (Fig. S7).

Comparison of FTIR spectrum of hydrothermal synthesized CuO, rGO and $CuO/rGO^{2:1}$ indicated the interaction between CuO and rGO in $CuO/rGO^{2:1}$ (Fig. 1b). The peaks at around 3442.37 cm^{-1} and 1643.08 cm^{-1} indicated adsorbed water. The C–O bond of epoxy and C═O bond or C═C bond in rGO were characterized by peaks detected at 1206.77 cm^{-1} and 1567.06 cm^{-1}, respectively [48]. The peaks appeared at 602.87 cm^{-1}, 520.11 cm^{-1} and 447.67 cm^{-1} were assigned to CuO [49]. This result indicates the successful preparation of CuO/rGO composite. The shift of peaks at 602.87 cm^{-1}, 520.11 cm^{-1}, and 447.67 cm^{-1} to those at 598.35 cm^{-1}, 528.54 cm^{-1}, and 433.28 cm^{-1} implied the interaction between CuO and rGO. The shift of peaks at 1567 cm^{-1} and 1206.77 cm^{-1} to those at 1552.46 cm^{-1} and 1218.81 cm^{-1} might correspond to the complexation between C═O, C–O and Cu [35]. The new peaks at 1124.68 cm^{-1} and 1091.53 cm^{-1} were assigned to the C–O bond of alkoxy [50], suggesting the formation of Cu–O–C bond. Therefore, it was proposed that the interaction between CuO and rGO was established by Cu–O–C bond.

BET results showed that the rGO prepared by hydrothermal method has considerable specific surface area of 320.13 $m^2 \cdot g^{-1}$, while CuO prepared by hydrothermal method has specific surface area of 3.139 $m^2 \cdot g^{-1}$. The rGO-modified CuO, i.e., $CuO/rGO^{2:1}$ has specific surface area of 56.093 $m^2 \cdot g^{-1}$, which improved the dispersity of CuO. Data of CuO/rGO with different mass ratios of CuO to GO precursor are provided in Supplementary material (Fig. S8).

In TGA procedure, the CuO/rGO was treated in oxygen atmosphere, GO and rGO were treated in nitrogen atmosphere. Results showed that more than 80% of CuO/rGO (w/w) was CuO, and oxygen content was more than 43.5% in GO and 23.5% in rGO (Fig. S9). Results indicated that rGO had been successfully reduced from GO, the high oxygen content of GO provided abundant growth sites for CuO and the residual oxygen in rGO improved the hydrophilic property of CuO/rGO.

3.2. Degradation of 2,4,6-trichlorophenol by CuO/rGO-PS system

3.2.1. Enhanced PS activation by CuO with rGO modification.

The contrast experiments were conducted among CuO/rGO-TCP, CuO/rGO-PS-TCP, $CuO/rGO^{acid\ wash}$-PS-TCP, CuO-PS-TCP, PS-TCP and Cu^{2+}-PS-TCP systems (Fig. 3). Results showed that CuO/rGO or PS had no removal capacity for TCP, while TCP concentration decreased significantly with CuO/rGO and PS together, which indicated that PS could be activated by CuO/rGO. Because of the low efficiency of TCP removal by the Cu^{2+}-PS system, the reaction was certainly heterogeneous process. CuO had been reported to be an efficient heterogeneous activator for PS, while in this study, the CuO-PS system showed a poor removal efficiency for TCP. This evidence revealed that rGO played a critical role in PS activation. Graphene is proved to be an efficient activator for PS [21,51–54]. While, as showed in Fig. 3, after dissolution of CuO, the remained rGO in CuO/rGO exhibited little removal efficiency for TCP, indicating that in the CuO/rGO composite the rGO content was too small (the dosage is 0.1 $g \cdot L^{-1}$, and wt.% of rGO is about 20%) to produce a significant TCP removal efficiency. There are research papers about TCP adsorption by graphene and graphene oxide [55,56], the adsorption test in this study showed that 0.1 g/L and 0.02 g/L rGO achieved 28% and 13% TCP removal rate in 0.1 $mmol \cdot L^{-1}$

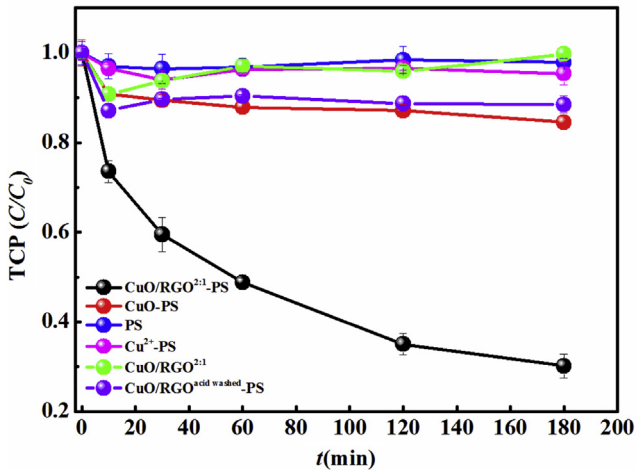

Fig. 3. Removal of TCP by different systems: CuO/rGO-TCP, CuO/rGO-PS-TCP, CuO/rGOacid wash-PS-TCP, CuO-PS, Cu^{2+}-PS and PS. The acid wash procedures were as follows: 0.01 g CuO/rGO were dispersed in 50 mL 0.2 M H_2SO_4 solution and shaken for 24 h. to remove supported CuO. Conditions: $[PS]_0$ = 2.5 mmol·L^{-1}, $[TCP]_0$ = 0.1 mmol·L^{-1}, [CuO/rGO] = 0.1 g·L^{-1}, [CuO] = 0.1 g·L^{-1}, [Cu^{2+}($CuSO_4$)] = 0.1 g·L^{-1}, No pH adjustment (about 2.8), T = 25 °C.

solution respectively, while nearly no TCP was removed by GO, indicating that adsorption effect is limited (Fig. S10). The TCP adsorption capacity of graphene is consistent with previous study [55], but the adsorption is not obvious because of the low content of rGO. As a conclusion, the interaction between rGO and CuO improved the surface activation ability of CuO for PS.

3.2.2. Effect of rGO content in CuO/rGO composite for PS activation and TCP removal

In this study, five kinds of CuO/rGO composites with different rGO contents were synthesized by controlling the mass ratio of CuO (calculated from $Cu(NO_3)_2{\cdot}3H_2O$) and GO precursor. They are CuO, CuO/$rGO^{10:1}$, CuO/$rGO^{4:1}$, CuO/$rGO^{2:1}$, and CuO/$rGO^{1:1}$. CuO/$rGO^{1:2}$, CuO/$rGO^{1:4}$, CuO/$rGO^{1:10}$ and CuO/$rGO^{1:20}$ were excluded because no CuO but Cu_2O was formed (as XRD results in Fig. S1). As shown in Fig. 4a, TCP removal efficiency increased with higher graphene content in the CuO and rGO composite. The higher rGO content provided more surface area for the CuO growth and led to a higher dispersity of CuO. Hence, the interaction between rGO and CuO was reinforced simultaneously, resulting in the better TCP removal efficiency. It indicated that CuO/$rGO^{1:1}$ has the best performance for TCP removal. Since CuO is our target and for cost-efficient application of material, CuO/$rGO^{2:1}$ with higher CuO content rather than CuO/$rGO^{1:1}$ was selected as PS activator in following study.

3.2.3. Effect of pH, CuO/$rGO^{2:1}$ dosage and persulfate concentration for TCP degradation

The pH would influence the surface electric property of material, protonation or deprotonation of a pollutant, and the dissolution of CuO. As shown in Fig. 4b, the best performance was achieved within pH 6 and 9. The pH was less than 3 if the system pH was not adjusted, and in this condition TCP could be degraded more efficiently than the condition with initial pH 11. The CuO corrosion became evident without pH adjustment (Cu^{2+} was 49.7 mg·L^{-1} after reaction). Therefore, the operation pH should be adjusted to near neutral, because in these conditions the TCP removal efficiency was highest and CuO corrosion was significantly inhibited (Cu^{2+} was 6.7 and 5.0 mg·L^{-1} after reaction at pH 6 and 9 respectively). In microcosmic perspective, the surface electric property of a material influences the adsorption of PS ion and pollutants. For this perspective, the zeta potential of CuO/rGO in solution has been tested and the values were −7.97 mV, −9.49 mV, −40.9 mV at pH 6, 9 and 11 respectively. Therefore, the surface charge of the composite would be most negative when pH is 11, which would have resulted in the maximum repulsion for PS anion, and further significant suppression of PS activation. When pH was 6–9, the less negative charge on the surface of composite resulted in less repulsion for PS anion, facilitating PS activation and TCP degradation. In an acidic condition, positive charge on the surface of composite would attract PS anion, hence TCP was still degraded in a large extent. While, the protonated TCP would be more difficult to be attracted to the surface of CuO, and the CuO corrosion decreased the active site on the surface (Cu^{2+} dissolution was 49.7 mg·L^{-1} after 180 min without pH adjustment in CuO/rGO-PS system), which limited the TCP degradation. To study the stability of CuO/rGO composite, the material was reused for three times. Results showed that the TCP degradation efficiency decreased when recycle time increased (Fig. S11). Considering the dissolution of Cu^{2+} is 6.7 ppm at pH 6, it is concluded that the loss of CuO have an obvious effect for persulfate activation and TCP removal. The SEM and TGA has been done for used CuO/rGO composite. The SEM results showed that the density of CuO particles on graphene are almost the same, indicating that the interaction between CuO and rGO is stable. The TGA results showed that CuO would dissolve in solution, the mass ratio of CuO in CuO/rGO decreased from 80% to 70%, indicating that the CuO faces the dissolution problem, which will be focused on in future work. The CuO dissolution in different systems are showed in Fig. S12, higher pH and lower PS concentration resulted in lower CuO dissolution.

CuO/$rGO^{2:1}$ dosage exhibited obvious effect to TCP removal (Fig. 4c). When dosage was raised from 0.05 g·L^{-1} to 0.1, the removal efficiency increased to three times. When dosage was further raised to 0.25 and 0.5 g·L^{-1}, TCP was completely removed in 60 min and 30 min, respectively. PS concentration also showed regular effect on TCP removal. There was no significant difference in TCP removal efficiency when PS concentration was raised from 1 mmol·L^{-1} to 5 (Fig. 4a); the calculated PS demand for complete mineralization was 1.1 mmol·L^{-1}. This result indicates that the active site on the CuO surface was close to saturation for PS when PS concentration was more than 1 mmol·L^{-1} (under the CuO/$rGO^{2:1}$ dosage of 0.1 g·L^{-1}). Therefore, keeping PS at 2.5 mmol·L^{-1} and increasing CuO/$rGO^{2:1}$ dosage would increase the active site, resulting in further increase of PS activation and TCP removal efficiency. When PS concentration was raised from 0 mmol·L^{-1} to 1 (Fig. 4a), TCP removal efficiency increased gradually; especially when PS concentration increased from 0 mmol·L^{-1} to 0.025 (low concentration, the molar ratio of TCP to PS is 4), the TCP removal efficiency increased obviously, indicating that PS play an important role in TCP degradation. It was concluded that higher CuO/$rGO^{2:1}$ dosage and PS concentration would increase the TCP removal efficiency. In addition, no inhibition was found at a high activator dosage or PS concentration, which was different from a typical radical-generating system [9].

The TOC removal has been investigated (Fig. S13). Results showed that about 30% TOC was removed by 0.1 g·L^{-1} CuO/rGO and 2.5 mmol·L^{-1} PS at pH 6 after 180 min. Compared with high TCP removal rate, it could be concluded that: 1) the TCP was degraded by activated PS but not adsorbed on CuO/rGO, because adsorption could cause the same removal rate of TOC and TCP; 2) the intermediate was not easy to be further degraded due to the low TOC removal rate but high TCP removal rate. When PS concentration was decreased to 1 mmol·L^{-1} and 0.5 mmol·L^{-1}, it was interesting to find that the TOC removal increased a little bit. A reasonable explanation is that: part of the intermediates would adsorbed on CuO/rGO, leading to the TOC removal in solution; when PS concentration increased, the adsorbed intermediates reacted with excess PS and released to solution again, the TOC in solution increased. The GC/MS analysis of adsorbed intermediates were 6-dichloro-2, 5-cyclohexadiene-1, 4-dione and 3, 5-dichloro-1, 2-Benzenediol. When CuO/rGO dosage increased to

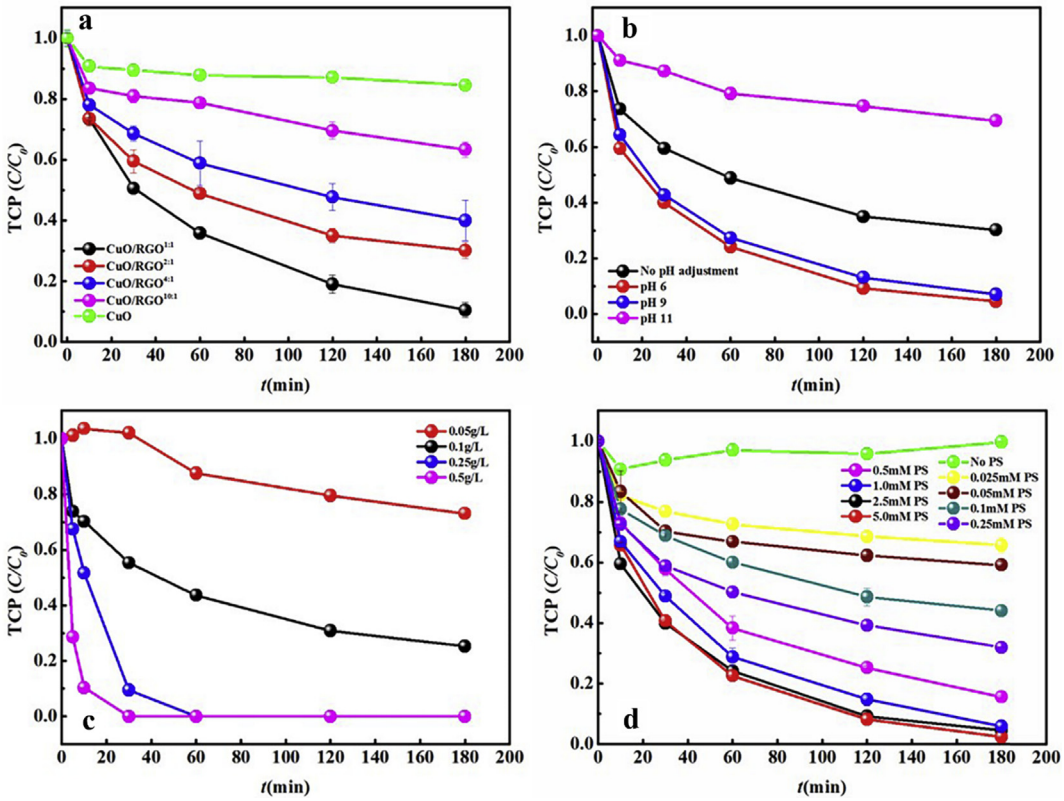

Fig. 4. (a) Effect of rGO content in CuO/rGO composite on TCP removal, conditions: $[PS]_0$ = 2.5 mmol·L^{-1}, $[TCP]_0$ = 0.1 mmol·L^{-1}, [CuO/rGO] = 0.1 g·L^{-1}, No pH adjustment (about 2.8), T = 25 °C; (b) Effect of pH on TCP degradation, conditions: $[PS]_0$ = 2.5 mmol·L^{-1}, $[TCP]_0$ = 0.1 mmol·L^{-1}, [CuO/rGO] = 0.1 g·L^{-1}, T = 25 °C; (c) Effect of CuO/rGO dosage on TCP degradation, conditions: $[PS]_0$ = 2.5 mmol·L^{-1}, $[TCP]_0$ = 0.1 mmol·L^{-1}, No pH adjustment (about 2.8), T = 25 °C; (d) Effect of persulfate concentration on TCP degradation, conditions: $[TCP]_0$ = 0.1 mmol·L^{-1}, [CuO/rGO] = 0.1 g·L^{-1}, pH 6, T = 25 °C.

0.25 g·L^{-1} and PS concentration increased to 5.0 mmol·L^{-1}, the TOC removal rate increased to 56.11%.

3.3. Reaction mechanism in CuO/rGO-PS-TCP system

3.3.1. Non-radical activation of PS by CuO/rGO

CuO has been reported as an activator of PS non-radical activation [28,29]. Evidences have also been discovered in this study. The decomposition of PS was researched in CuO/rGO-PS system and nearly no consumption of PS happened, while when pollutant 4-chloroaniline was added in CuO/rGO-PS system, obvious decomposition of PS was observed, indicating the non-radical PS activation process for pollutant degradation (Fig. 5a). Nearly no inhibition of TCP removal rate was found in the presence of ethanol ($k_{OH}\cdot$ = 1.2–2.8 × 10^9 M^{-1} S^{-1}, $k_{SO4}{}^{-}\cdot$ = 1.6–7.7 × 10^7 M^{-1} S^{-1} [57]) or isopropanol ($k_{OH}\cdot$ = 1.9 × 10^9 M^{-1} S^{-1} [58], $k_{SO4}{}^{-}\cdot$ = 8.7 × 10^7 M^{-1} S^{-1} [59]) as a radical scavenger (Fig. 5b), further proved the non-radical activation mechanism. To directly detect radicals, electron paramagnetic resonance has been applied. As shown in Fig. 10a, sulfate and hydroxyl radicals were produced in CuO/rGO-PS (Fig. 5c), in accordance with our previous study [29]. Interestingly, the radical signal intensity in the CuO/rGO-PS system was weaker than that in the Cu^{2+}-PS system (Fig. 5d), while TCP removal efficiency in the CuO/rGO-PS system was higher than that in the Cu^{2+}-PS system. The result indicated that sulfate and hydroxyl radicals were not main reactive oxygen species. It was reasonably to suppose that activated PS was the main PS activation products in CuO/rGO. The radicals might be generated during PS activation by dissolved Cu^{2+} and strong active site on CuO [29].

3.3.2. Non-radical activation site on CuO/rGO

Persulfate activation by CuO/rGO has been proved to be a non-radical process, and this process has been reported to occur on the CuO surface [28,29]. Zhang et al. [28] used O_2 adsorption method to determine the Cu atom density on CuO surface and establish the quantitative relation between reaction rate and Cu content on surface. Du et al. [29] studied on the reusability of CuO, the results showed that Cu density on CuO and the performance of CuO both decreased after used. These two studies both indicated that Cu atom was probably the active site for persulfate activation. Further experiment was designed to find more evidence for active site on CuO surface. Sulfhydrylization reagents 4-mercaptobenzoic acid, dimercaprol and 3-mercaptopropionic were used to block copper atom on CuO surface by complexation between Cu atoms and sulfydryl group (Fig. S14). After surface modification, TCP removal by CuO/rGO-PS was significantly inhibited (Fig. 6a). The dimercaprol was most efficient in suppressing TCP degradation, followed by 4-mercaptobenzoic acid and 3-mercaptopropionic. The results indicated that copper atom on surface was active site for persulfate activation, the complex formed between Cu and persulfate on surface without radical generation. In conclusion, the non-radical activation process was occurred on copper atoms of CuO surface.

It was reported that a high electron density around Cu could be achieved by Cu–O–C bond interaction between Cu-containing oxide and typical π-conjugated graphitic planes of g-C_3N_3, which is efficient in H_2O_2 activation to generate hydroxyl radicals [35], indicating that electron-rich center would be a good activator. Graphene also contained π-conjugated graphitic planes, hence it was reasonable to propose the electron-rich center on CuO. FTIR results confirmed the formation of Cu–O–C bond, which established the interaction between CuO and rGO. In literature, it has been proved that electron transfer from g-C_3N_3 to a supported material happened through the Cu–O–C bond, resulting in the electron-rich center on the supported material and the electron-deficient center on g-C_3N_3 [35]. The same

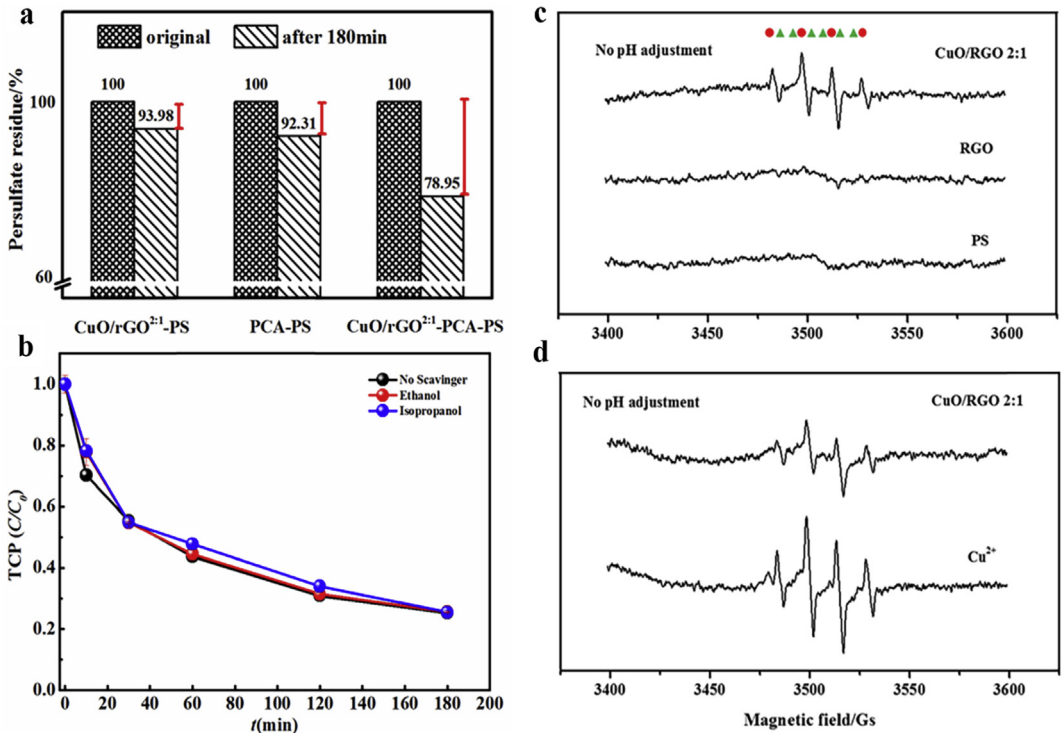

Fig. 5. (a) Persulfate decomposition in CuO/rGO-PS, PCA-PS and CuO/rGO-PCA-PS systems, conditions: $[PS]_0 = 2.5\ mmol{\cdot}L^{-1}$, $[PCA] = 0.5\ mmol{\cdot}L^{-1}$, $[CuO/rGO] = 0.1\ g{\cdot}L^{-1}$, pH = 6, T = 25 °C; (b) Effect of sulfate and hydroxyl radical scavengers on TCP removal by CuO/rGO system, conditions: $[PS]_0 = 2.5\ mmol{\cdot}L^{-1}$, $[TCP]_0 = 0.1\ mmol{\cdot}L^{-1}$, $[CuO/rGO] = 0.1\ g{\cdot}L^{-1}$, $[ethanol]_0 = 100\ mmol{\cdot}L^{-1}$, $[isopropanol]_0 = 100\ mmol{\cdot}L^{-1}$, No pH adjustment (about 2.8), T = 25 °C; (c) and (d) Radical detection by EPR in CuO/rGO-PS, rGO-PS, Cu^{2+}-PS and PS solution systems. The red circles stand for hydroxyl radical and green triangles stand for sulfate radical. Conditions: $[PS]_0 = 2.5\ mmol{\cdot}L^{-1}$, $[CuO/rGO] = 0.1\ g{\cdot}L^{-1}$, $[rGO] = 0.02\ g{\cdot}L^{-1}$, $[Cu^{2+}(CuSO_4)] = 0.1\ g{\cdot}L^{-1}$, No pH adjustment (about 2.8), T = 25 °C.

circumstance in CuO/rGO might also exist. By forming the electron-rich center on CuO, PS was more easily activated on CuO surface. The significantly enhanced TCP removal rate in the CuO/rGO-PS system than in the CuO-PS system supported the possibility of an electron-rich center formation. Furthermore, electron paramagnetic resonance was applied to prove the existence of an electron-rich center. In the study of Lyu et al. [35], the electron-rich center activated H_2O_2 to be hydroxyl radicals. In this study, the results showed that hydroxyl and superoxide radicals were formed in both CuO/rGO-H_2O_2 and CuO-H_2O_2 systems (Fig. 6b). While the radical signal had no obvious difference. Moreover, the unexpected superoxide radical appeared (The formed superoxide radical probably resulted from photocatalysis by indoor light) and the preconceived hydroxyl radical signal was not significant. The results indicated that the electron-rich center was too weak to activate H_2O_2 to be radicals. Therefore the weak electron-rich center might activate PS by non-radical processes. In conclusion, the interaction between CuO and rGO was not strong enough to activate H_2O_2 to form radicals but enhanced the PS non-radical activation.

3.4. Crystal facet effect of CuO for PS activation

Besides the enhancement of PS activation by rGO, CuO could also be self-enhanced by exposing different surface. Crystal facet effect always exists in a heterogeneous catalysis reaction, resulting in different reaction ability of a catalyst; the surface on a differently exposed crystal facet would exhibit distinguishable active sites [36]. Saputra et al.

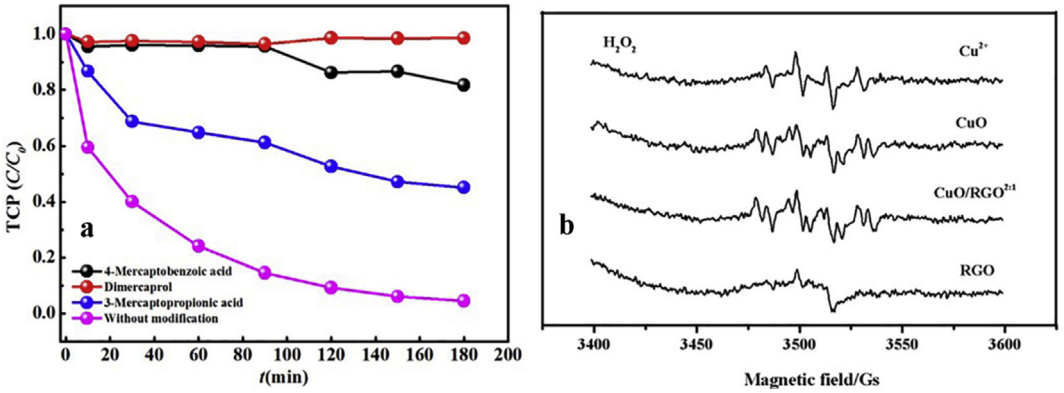

Fig. 6. (a) TCP removal in CuO/rGO-PS system after surface copper atom block, conditions: $[PS]_0 = 2.5\ mmol{\cdot}L^{-1}$, $[TCP]_0 = 0.1\ mmol{\cdot}L^{-1}$, $[CuO/rGO] = 0.1\ g{\cdot}L^{-1}$, pH = 6, T = room temperature; (b) Radical detection by EPR in CuO/rGO-H_2O_2, CuO-H_2O_2, rGO-H_2O_2 and Cu^{2+}–H_2O_2 system, conditions: $[H_2O_2]_0 = 2.5\ mmol{\cdot}L^{-1}$, $[CuO] = 0.1\ g{\cdot}L^{-1}$, $[CuO/rGO] = 0.1\ g{\cdot}L^{-1}$, $[Cu^{2+}(CuSO_4)] = 0.1\ g{\cdot}L^{-1}$, No pH adjustment (about 2.8), T = 25 °C.

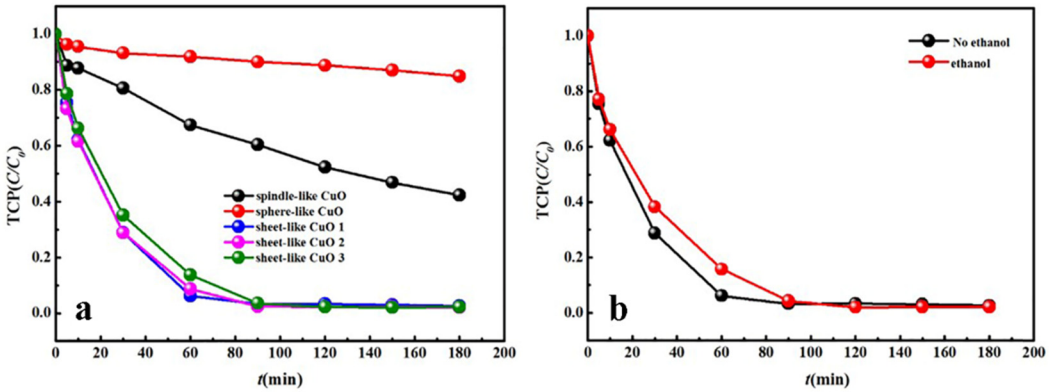

Fig. 7. (a) Effect of crystal facet (morphology) on TCP removal by CuO-PS system. CuO 1 was prepared without PEG200, CuO 2 was prepared with 2 mL PEG200, CuO 3 was prepared with 10 mL PEG200. (b) Effect of radical scavenger ethanol on TCP removal by sheet-like CuO-PS system. Conditions: $[PS]_0$ = 2.5 mmol·L^{-1}, $[TCP]_0$ = 0.1 mmol·L^{-1}, [CuO] = 0.1 g·L^{-1}, [ethanol] = 100 mmol·L^{-1}, pH = 6, T = 25 °C.

[60,61] studied the shape selective reaction between peroxymonosulfate and single transition oxide like Mn_2O_3 and Co_3O_4 for phenol degradation, the results showed that the more reactive surface facet play an important role in catalysis. Therefore it is necessary to investigate the effect of exposed surface for reaction. In this study, we have investigated three kinds of CuO with different morphology prepared from three methods, the spindle-like CuO by the high temperature hydrothermal method, the sphere-like CuO by calcination and the sheet-like CuO by the low temperature hydrothermal method. Results showed that sheet-like CuO resulted in significantly efficient TCP degradation, while spindle-like CuO resulted in moderate TCP removal efficiency and sphere-like CuO resulted in weak TCP removal (Fig. 7a, Table S1). The apparent pseud-first order reaction rate constant for sheet-like CuO is 60 times and 10 times of that for sphere-like and spindle-like CuO respectively. It is noted that the specific surface area of sheet-like, sphere-like and spindle-like CuO is 13 [37], 0.96 [28] and 3.14 $m^2 \cdot g^{-1}$ respectively. After the normalization of rate constant by specific surface area (Table S2), the pseud-first order reaction rate constant for sheet-like CuO is 4.5 times and 2.4 times of that for sphere-like and spindle-like CuO respectively. The facts indicated that surface facet had a great impact on PS activation. The HRTEM results in Fig. 8 revealed that the main exposed crystal facet of the sheet-like CuO was (0 0 1), in accordance with the previously reported result [62]. The (0 0 2) facet took up a small ratio of the sphere-like CuO surface. While the polycrystalline (as shown by SAED results in Fig. 8c) spindle-like CuO was formed from particles aggregation, and the particles growth direction was random, which means that the exposed crystal facets can cover all the possible crystal facets [63]. Therefore, the (0 0 1) facet was efficient in PS activation. Further experiments proved that the activation was non-radical process (Fig. 7b). By analyzing the atomic occupancy on the surface (the exposed atoms on (0 0 1) surface were all Cu), it was concluded that a higher copper site content can result in higher PS activation, indicating that copper atom on surface was the persulfate activation site. To verify the speculation, three sulfhydryl compounds were used to block the copper site on the CuO surface (part 3.3.2). As expected, the thiol-modified CuO/rGO significantly inhibited TCP degradation, confirming the speculation that copper atom on the CuO surface was PS activation site. Therefore, CuO had crystal facet effect on PS activation and copper atom on the surface was the PS activation site, the facet (0 0 1) with a higher copper site content on the surface was efficient. The exposed facet identification procedure was shown in Supplementary material (Text 4).

3.5. Selective removal of organic pollutants by non-radical CuO/rGO-PS system

3.5.1. Selective removal of different chlorinated organic pollutants

Radical oxidation system like Fenton or PS based systems always showed high removal efficiency for a wide spectrum of organic pollutants. However, the radical oxidation systems demand excess amount of oxidants and catalysts for complete removal of target pollutants in the presence of other non-target pollutants. A non-radical oxidation system does not require an overactive radical, allowing PS to react with pollutants in a more stable condition.

Pollutant-selective-oxidation property of the CuO/rGO-PS system was studied in three aspects: degradation distinction of chlorophenols with different number (1–3) of chloride as a substituent, degradation distinction of chloride benzene with amido and phenolic hydroxyl group, and degradation distinction of chloride organics with benzene ring and double bond of carbon.

As shown in Fig. 9, it was easier to degrade the chlorophenol with more chlorides, chlorinated benzene with amido, and chlorinated organics with benzene ring. In first aspect, degradation of TCP, DCP and CP has been investigated at pH 2.8, 6, 9 and 11. The removal efficiency followed the sequence of TCP > DCP > CP, TCP > DCP > CP, TCP > DCP > CP and CP > DCP > TCP at pH pH 2.8, 6, 9 and 11, respectively. At pH 2.8 to 9, TCP could be easily degraded, while in basic condition (pH 11), the degradation was significantly inhibited. Considering the zeta potential of CuO/rGO in solution and pK_a of three chlorophenols (i.e., 6.59, 8.05, and 9.47 for TCP, DCP, and CP, respectively), it could be concluded that when pH was 11, the CuO surface was most negatively charged and the repulsion between the surface and TCP was significant, since the distinction between pK_a of TCP and pH was more than that between pK_a of DCP or CP and pH. Therefore, the reaction activity between the surface and TCP was inhibited.

The selective oxidation sequence of chlorophenols by the CuO/rGO-PS system was TCP > DCP > CP. In second aspect, degradation of 4-chlorophenol and 4-chloroaniline was investigated at pH 2.8, 6, 9 and 11. In short, PCA was much more easily degraded than CP. Even at pH 11, the condition that was most beneficial for CP and most unfavorable for PCA, removal efficiencies of the system for CP and PCA were comparable. It could be concluded that amido and phenolic hydroxyl group exhibited different effect on chlorinated benzene ring. Since the electron-donating ability of $–NH_2$ was stronger than that of –OH, it was proposed that the benzene-ring-conjugated system affected by $–NH_2$ might be more reactive than that affected by –OH.

In third aspect, degradation of 2,4,6-trichlorophenol (TCP) and trichloroethylene (TCE) were investigated at pH 2.8, 6, 9 and 11 (Fig. S15). Results showed that TCP was more easily degraded than TCE except the pH 11 condition, and pH adjustment had nearly no effect for

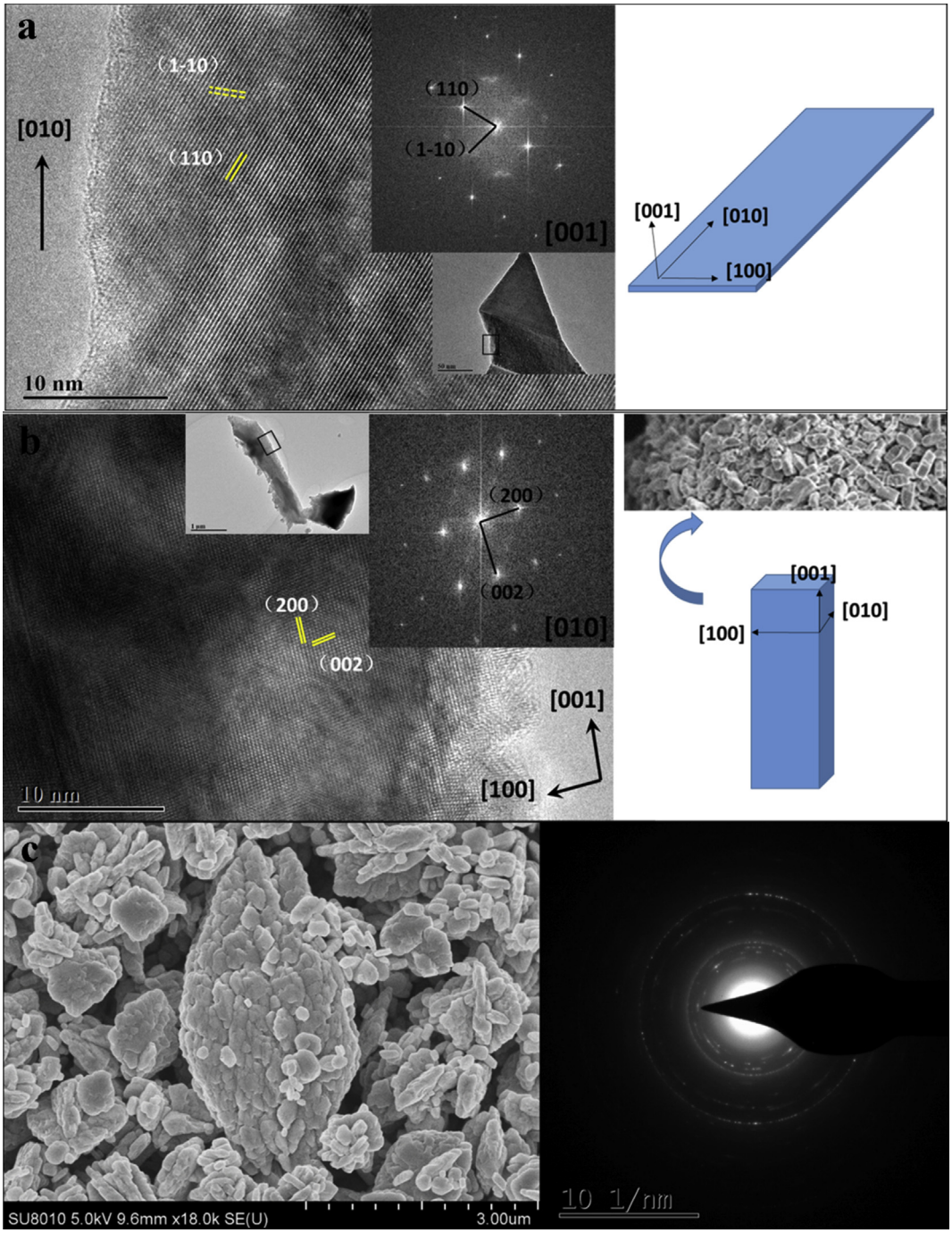

Fig. 8. TEM and SEM results of CuO, (a) HRTEM and FFT of sheet-like CuO, (b) HRTEM and FFT of sphere-like CuO, (c) SEM and SAED of spindle-like CuO.

TCE degradation. Since benzene ring conjugated system has higher electron cloud density than double bond of carbon, TCP would be a better electron donator than TCE, which accounted for higher reactivity of TCP.

In conclusion, CuO/rGO-PS system showed a good selective oxidation ability for chlorophenols with different chloride number, for chloride benzene with different substituent group, and for organics with different unsaturation carbon bond. The conclusion showed the advantage of persulfate non-radical activation system for focusing on target pollutants with less impact from impurities, compared with omnipotent radical-generated system. The rate constants and removal rate of different pollutants are showed in Table S3.

3.5.2. Dechlorination of TCP and intermediates identification

Experiments have demonstrated the high efficiency of TCP removal in CuO/rGO-PS system. To evaluate the TCP degradation characteristic in this non-radical system, dechlorination degree and intermediates have been studied. Compared with typical radical-generated system Fe^0-PS, chloride ion concentration in CuO/rGO-PS system first increased and then became stable, which was in accordance with TCP degradation tendency (Fig. S16). While in Fe^0-PS system, chloride ion concentration first increases and then decreased, which was probably due to the chloride radical formation from chloride ion oxidation by sulfate radical. Therefore the activated persulfate in CuO/rGO-PS system was not active enough for chloride ion oxidation, increasing the selective oxidation ability for pollutants and avoiding the polychlorinated organics. To study the TCP dechlorination efficiency,

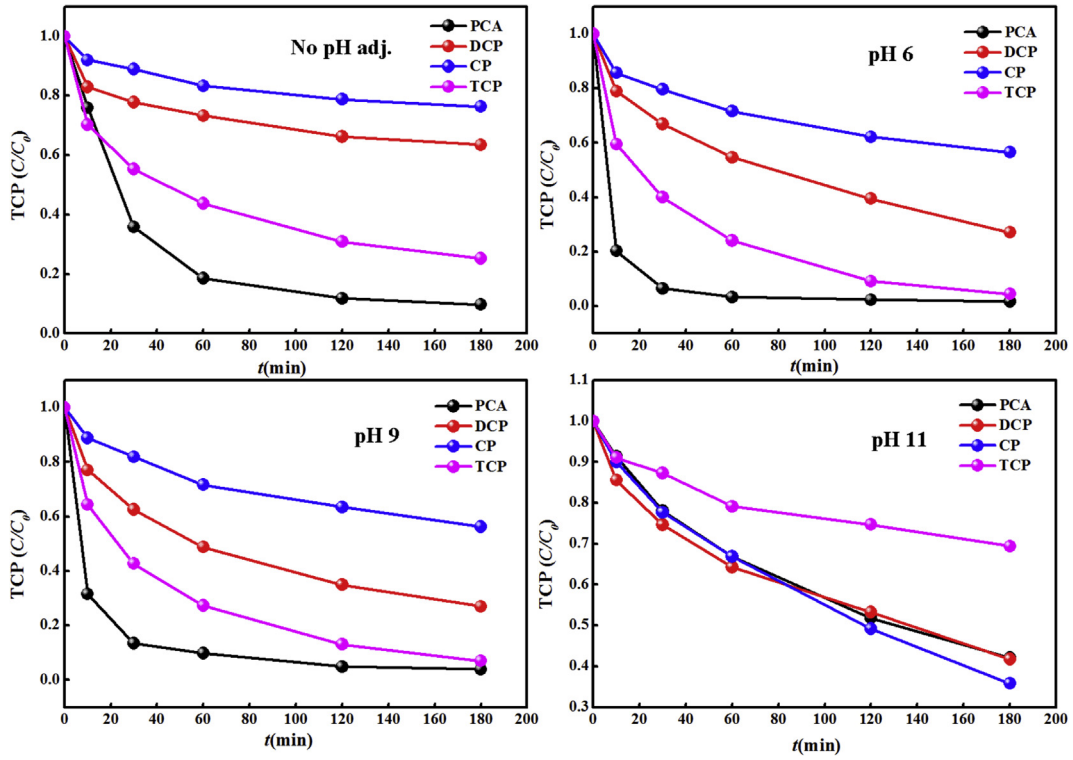

Fig. 9. Selective removal of different pollutants by CuO/rGO system. Conditions: $[PS]_0$ = 2.5 mmol·L^{-1}, [CuO/rGO] = 0.1 g·L^{-1}, $[TCP]_0$ = 0.1 mmol·L^{-1}, $[DCP]_0$ = 0.1 mmol·L^{-1}, $[CP]_0$ = 0.1 mmol·L^{-1}, $[PCA]_0$ = 0.1 mmol·L^{-1}, T = 25 °C.

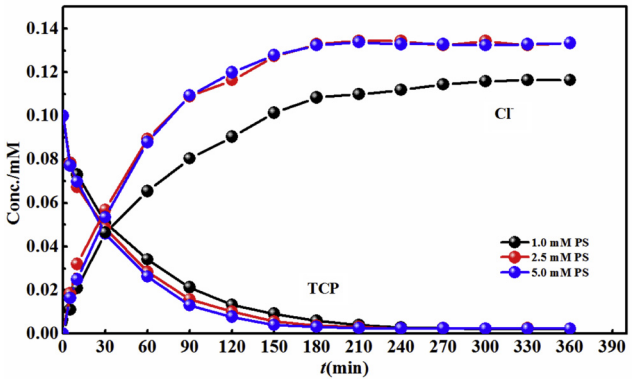

Fig. 10. Effect of persulfate concentration on TCP dechlorination by CuO/rGO system. Conditions: $[TCP]_0$ = 0.1 mmol·L^{-1}, [CuO/rGO] = 0.1 g·L^{-1}, pH = 6, T = 25 °C.

persulfate concentration was investigated (Fig. 10). Results showed that when persulfate concentration increased from 1 mmol·L^{-1} to 2.5 mmol·L^{-1}, chloride ion content increased mildly. When persulfate concentration further increased from 2.5 mmol·L^{-1} to 5 mmol·L^{-1}, almost no increase of chloride ion content happened. Considering the molar ratio of final chloride ion to TCP, it was proposed that about 100 TCP molecules lost 116, 133 and 133 chloride atom when persulfate concentration was 1, 2.5 and 5 mmol·L^{-1} respectively, most TCP molecule just lost one chloride atom and part TCP molecule lost two or three, the identified 2, 6-dichloro-2, 5-cyclohexadiene-1, 4-dione and 3, 5-dichloro-1, 2-Benzenediol intermediates verified the speculation (Fig. S17). It was concluded that TCP molecule easily lost one chloride during oxidation processes in CuO/rGO-PS system (equation 1), and the dechlorinated intermediates was difficult to be oxidized compared with TCP, which was consistent with low TOC removal rate, reflecting the selective oxidation property of CuO/rGO-PS system. The persulfate decomposition was also studied (Fig. S18) to verify TCP degradation pathway. According to the equation, one persulfate molecule could transform two TCP molecules, indicating that 0.1 mmol TCP degradation only needs only 0.05 mmol persulfate theoretically. When initial TCP and persulfate concentration is 0.1 mmol/L and 1.0 mmol/L respectively, the persulfate consumption is about 5% or more. The PS decomposition line is showed in Fig. S18, about 13% persulfate is consumed in CuO/rGO-PS-TCP system, while it is about 10% in CuO/rGO-PS and nearly no persulfate is consumed in PS-TCP system. This phenomenon indicated that interaction between persulfate and CuO/rGO happens and TCP addition increases persulfate decomposition. The persulfate decreases more and more slowly in CuO/rGO-PS, indicating that persulfate is probably adsorbed on CuO/rGO. When TCP is introduced, more persulfate is consumed and shows continuous consumption. The results proved that persulfate would be adsorbed on CuO/rGO surface without radical generation and continuous consumption, and persulfate oxidizes TCP by dechlorination pathway.

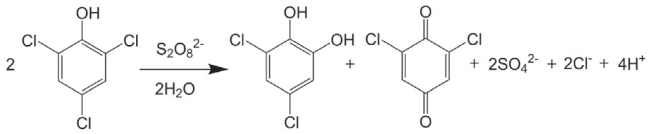

Equation 1. The main processes of TCP degradation in CuO/rGO-PS-TCP system.

4. Conclusion

Copper oxide activates persulfate by non-radical generation process. Hydrothermal synthesized CuO/rGO could efficiently activate persulfate and completely remove 2,4,6-trichlorophenol in aqueous under experiment condition. According to the results, the rGO enhanced the persulfate activation ability of CuO significantly. The CuO/rGO-PS system showed good selectivity degradation for various chlorinated organic pollutants, exhibiting the advantage for specific pollutant removal, compared with non-selective radical oxidation systems. By applying the non-radical activation system, 4-chloroaniline was most

easily degraded, followed by 2,4,6-trichlorophenol, 2,4-dichlorophenol and 4-chlorophenol, under acidic, neutral and weak basic condition (pH 3–9). Furthermore, pollutants with benzene ring was more reactive than that with double bond of carbon in the system. Different exposed crystal facet of CuO showed different persulfate activation efficiency, specifically the facet (0 0 1) was most efficient. In conclusion, the non-radical activation system showed good selectivity of organic pollutants degradation, and CuO could be enhanced by reduced graphene oxide and tunable exposed crystal facet, resulting in higher and tunable persulfate activation ability. Note that the dissolution of CuO, measurements should be adopted to inhibited the second pollution and improve the stability of material. Since the TCP was mainly oxidized but not adsorbed, and not high TOC removal was achieved, the toxicity and biodegradation of the effluent during reaction processes should be studied in future work.

Acknowledgements

This work was financially supported by the National Natural Science Foundation of China (51572089, U1701243), the National Key Research and Development Program of China, China (2016YFC0400708), the Natural Science Foundation of Guangdong Province, China (2015A030313232), the Foundation of Science and Technology Planning Project of Guangdong Province, China (2016A050502007), the Foundation of Science and Technology Planning Project of Guangzhou, China (201804010398) and the Funds of State Key Laboratory of Pulp and Paper Engineering (201837).

Appendix A. Supplementary data

Supplementary data associated with this article can be found, in the online version, at https://doi.org/10.1016/j.cej.2018.08.216.

References

[1] S. Wacławek, H.V. Lutze, K. Grübel, V.V.T. Padil, M. Černík, D.D. Dionysiou, Chemistry of persulfates in water and wastewater treatment: a review, Chem. Eng. J. 330 (2017) 44–62.
[2] W. Li, R. Orozco, N. Camargos, H. Liu, Mechanisms on the impacts of alkalinity, pH, and chloride on persulfate-based groundwater remediation, Environ. Sci. Technol. 51 (2017) 3948–3959.
[3] P. Devi, U. Das, A.K. Dalai, In-situ chemical oxidation: principle and applications of peroxide and persulfate treatments in wastewater systems, Sci. Total Environ. 571 (2016) 643–657.
[4] L.W. Matzek, K.E. Carter, Activated persulfate for organic chemical degradation: a review, Chemosphere 151 (2016) 178–188.
[5] W.-D. Oh, Z. Dong, T.-T. Lim, Generation of sulfate radical through heterogeneous catalysis for organic contaminants removal: current development, challenges and prospects, Appl. Catal., B 194 (2016) 169–201.
[6] B.-T. Zhang, Y. Zhang, Y. Teng, M. Fan, Sulfate radical and its application in decontamination technologies, Crit. Rev. Environ. Sci. Technol. 45 (2015) 1756–1800.
[7] F.C. Moreira, R.A.R. Boaventura, E. Brillas, V.J.P. Vilar, Electrochemical advanced oxidation processes: a review on their application to synthetic and real wastewaters, Appl. Catal., B 202 (2017) 217–261.
[8] Z. Wei, F.A. Villamena, L.K. Weavers, Kinetics and mechanism of ultrasonic activation of persulfate: an in situ EPR spin trapping study, Environ. Sci. Technol. 51 (2017) 3410–3417.
[9] I. Hussain, Y.Q. Zhang, S.B. Huang, X.Z. Du, Degradation of p-chloroaniline by persulfate activated with zero-valent iron, Chem. Eng. J. 203 (2012) 269–276.
[10] T. Zhou, X. Zou, J. Mao, X. Wu, Decomposition of sulfadiazine in a sonochemical Fe0-catalyzed persulfate system: parameters optimizing and interferences of wastewater matrix, Appl. Catal., B 185 (2016) 31–41.
[11] I. Hussain, M. Li, Y. Zhang, Y. Li, S. Huang, X. Du, G. Liu, W. Hayat, N. Anwar, Insights into the mechanism of persulfate activation with nZVI/BC nanocomposite for the degradation of nonylphenol, Chem. Eng. J. 311 (2017) 163–172.
[12] C. Cai, J. Liu, Z. Zhang, Y. Zheng, H. Zhang, Visible light enhanced heterogeneous photo-degradation of Orange II by Zinc ferrite (ZnFe2O4) catalyst with the assistance of persulfate, Sep. Purif. Technol. 165 (2016) 42–52.
[13] Y. Ding, L. Zhu, N. Wang, H. Tang, Sulfate radicals induced degradation of tetrabromobisphenol A with nanoscaled magnetic $CuFe_2O_4$ as a heterogeneous catalyst of peroxymonosulfate, Appl. Catal., B 129 (2013) 153–162.
[14] G.-D. Fang, D.D. Dionysiou, S.R. Al-Abed, D.-M. Zhou, Superoxide radical driving the activation of persulfate by magnetite nanoparticles: Implications for the degradation of PCBs, Appl. Catal., B 129 (2013) 325–332.
[15] H. Liu, T.A. Bruton, W. Li, J. Van Buren, C. Prasse, F.M. Doyle, D.L. Sedlak, Oxidation of benzene by persulfate in the presence of Fe(III)- and Mn(IV)-containing oxides: stoichiometric efficiency and transformation products, Environ. Sci. Technol. 50 (2016) 890–898.
[16] J. Yan, Y. Chen, L. Qian, W. Gao, D. Ouyang, M. Chen, Heterogeneously catalyzed persulfate with a CuMgFe layered double hydroxide for the degradation of ethylbenzene, J. Hazard. Mater. 338 (2017) 372–380.
[17] A.L. Teel, M. Ahmad, R.J. Watts, Persulfate activation by naturally occurring trace minerals, J. Hazard. Mater. 196 (2011) 153–159.
[18] D. Xia, Y. Li, G. Huang, R. Yin, T. An, G. Li, H. Zhao, A. Lu, P.K. Wong, Activation of persulfates by natural magnetic pyrrhotite for water disinfection: efficiency, mechanisms, and stability, Water Res. 112 (2017) 236–247.
[19] Y. Zhang, T. Hien Phuong, X. Du, I. Hussain, S. Huang, S. Zhou, W. Wen, Efficient pyrite activating persulfate process for degradation of p-chloroaniline in aqueous systems: a mechanistic study, Chem. Eng. J. 308 (2017) 1112–1119.
[20] X.G. Duan, H.Q. Sun, J. Kang, Y.X. Wang, S. Indrawirawan, S.B. Wang, Insights into heterogeneous catalysis of persulfate activation on dimensional-structured nanocarbons, ACS Catal. 5 (2015) 4629–4636.
[21] L. Bekris, Z. Frontistis, G. Trakakis, L. Sygellou, C. Galiotis, D. Mantzavinos, Graphene: a new activator of sodium persulfate for the advanced oxidation of parabens in water, Water Res. 126 (2017) 111–121.
[22] Y. Guo, Z. Zeng, Y. Zhu, Z. Huang, Y. Cui, J. Yang, Catalytic oxidation of aqueous organic contaminants by persulfate activated with sulfur-doped hierarchically porous carbon derived from thiophene, Appl. Catal., B 220 (2018) 635–644.
[23] S. Yang, X. Yang, X. Shao, R. Niu, L. Wang, Activated carbon catalyzed persulfate oxidation of Azo dye acid orange 7 at ambient temperature, J. Hazard. Mater. 186 (2011) 659–666.
[24] X. Cheng, H. Guo, Y. Zhang, X. Wu, Y. Liu, Non-photochemical production of singlet oxygen via activation of persulfate by carbon nanotubes, Water Res. 113 (2017) 80–88.
[25] X. Duan, C. Su, L. Zhou, H. Sun, A. Suvorova, T. Odedairo, Z. Zhu, Z. Shao, S. Wang, Surface controlled generation of reactive radicals from persulfate by carbocatalysis on nanodiamonds, Appl. Catal., B 194 (2016) 7–15.
[26] G. Fang, C. Liu, J. Gao, D.D. Dionysiou, D. Zhou, Manipulation of persistent free radicals in biochar to activate persulfate for contaminant degradation, Environ. Sci. Technol. 49 (2015) 5645–5653.
[27] X. Duan, Z. Ao, L. Zhou, H. Sun, G. Wang, S. Wang, Occurrence of radical and nonradical pathways from carbocatalysts for aqueous and nonaqueous catalytic oxidation, Appl. Catal., B 188 (2016) 98–105.
[28] T. Zhang, Y. Chen, Y. Wang, J. Le Roux, Y. Yang, J.-P. Croué, Efficient peroxydisulfate activation process not relying on sulfate radical generation for water pollutant degradation, Environ. Sci. Technol. 48 (2014) 5868–5875.
[29] X. Du, Y. Zhang, I. Hussain, S. Huang, W. Huang, Insight into reactive oxygen species in persulfate activation with copper oxide: activated persulfate and trace radicals, Chem. Eng. J. 313 (2017) 1023–1032.
[30] H. Lee, H.J. Lee, J. Jeong, J. Lee, N.B. Park, C. Lee, Activation of persulfates by carbon nanotubes: oxidation of organic compounds by nonradical mechanism, Chem. Eng. J. 266 (2015) 28–33.
[31] E.-T. Yun, H.-Y. Yoo, H. Bae, H.-I. Kim, J. Lee, Exploring the role of persulfate in the activation process: radical precursor versus electron acceptor, Environ. Sci. Technol. 51 (2017) 10090–10099.
[32] Y. Yang, J.J. Pignatello, J. Ma, W.A. Mitch, Comparison of halide impacts on the efficiency of contaminant degradation by sulfate and hydroxyl radical-based advanced oxidation processes (AOPs), Environ. Sci. Technol. 48 (2014) 2344–2351.
[33] Y. Wang, J. Le Roux, T. Zhang, J.-P. Croué, Formation of brominated disinfection byproducts from natural organic matter isolates and model compounds in a sulfate radical-based oxidation process, Environ. Sci. Technol. 48 (2014) 14534–14542.
[34] C. Guan, J. Jiang, C. Luo, S. Pang, C. Jiang, J. Ma, Y. Jin, J. Li, Transformation of iodide by carbon nanotube activated peroxydisulfate and formation of iodoorganic compounds in the presence of natural organic matter, Environ. Sci. Technol. 51 (2017) 479–487.
[35] L. Lyu, L. Zhang, G. He, H. He, C. Hu, Selective H2O2 conversion to hydroxyl radicals in the electron-rich area of hydroxylated C-g-C_3N_4/CuCo-Al_2O_3, J. Mater. Chem. A 5 (2017) 7153–7164.
[36] K. Zhou, Y. Li, Catalysis based on nanocrystals with well-defined facets, Angew. Chem. Int. Ed. 51 (2012) 602–613.
[37] J. Liu, J. Jin, Z. Deng, S.Z. Huang, Z.Y. Hu, L. Wang, C. Wang, L.H. Chen, Y. Li, G.V. Tendeloo, Tailoring CuO nanostructures for enhanced photocatalytic property, J. Colloid Interface Sci. 384 (2012) 1–9.
[38] M.M. Mekonnen, A.Y. Hoekstra, Four billion people facing severe water scarcity, Sci. Adv. 2 (2016) e1500323.
[39] M.M. Häggblom, I.D. Bossert, Halogenated organic compounds – a global perspective, in: M.M. Häggblom, I.D. Bossert (Eds.), Dehalogenation: Microbial Processes and Environmental Applications, Kluwer Academic Publishers, Boston, Mass, 2003.
[40] A.O. Olaniran, E.O. Igbinosa, Chlorophenols and other related derivatives of environmental concern: properties, distribution and microbial degradation processes, Chemosphere 83 (2011) 1297–1306.
[41] ATSDR, Comprehensive Environmental Response, Compensation, and Liability Act (CERCLA) Priority List of Hazardous Substances, (2007).
[42] M. Czaplicka, Sources and transformations of chlorophenols in the natural environment, Sci. Total Environ. 322 (2004) 21–39.
[43] National Toxicology Program, 2,4,6-Trichlorophenol, Report on carcinogens: carcinogen profiles 12 (2011) 424-426.
[44] J. Gao, L. Liu, X. Liu, H. Zhou, S. Huang, Z. Wang, Levels and spatial distribution of chlorophenols 2,4-dichlorophenol, 2,4,6-trichlorophenol, and pentachlorophenol in surface water of China, Chemosphere 71 (2008) 1181–1187.

[45] D.C. Marcano, D.V. Kosynkin, J.M. Berlin, A. Sinitskii, Z. Sun, A. Slesarev, L.B. Alemany, W. Lu, J.M. Tour, Improved synthesis of graphene oxide, ACS Nano 4 (2010) 4806–4814.
[46] C. Liang, C.F. Huang, N. Mohanty, R.M. Kurakalva, A rapid spectrophotometric determination of persulfate anion in ISCO, Chemosphere 73 (2008) 1540–1543.
[47] Z.-Y. Sui, B.-H. Han, Effect of surface chemistry and textural properties on carbon dioxide uptake in hydrothermally reduced graphene oxide, Carbon 82 (2015) 590–598.
[48] W. Chen, L. Yan, P.R. Bangal, Preparation of graphene by the rapid and mild thermal reduction of graphene oxide induced by microwaves, Carbon 48 (2010) 1146–1152.
[49] B. Zhao, P. Liu, H. Zhuang, Z. Jiao, T. Fang, W. Xu, B. Lu, Y. Jiang, Hierarchical self-assembly of microscale leaf-like CuO on graphene sheets for high-performance electrochemical capacitors, J. Mater. Chem. A 1 (2013) 367–373.
[50] M. Acik, G. Lee, C. Mattevi, A. Pirkle, R.M. Wallace, M. Chhowalla, K. Cho, Y. Chabal, The role of oxygen during thermal reduction of graphene oxide studied by infrared absorption spectroscopy, J. Phys. Chem. C 115 (2011) 19761–19781.
[51] X. Duan, H. Sun, Z. Shao, S. Wang, Nonradical reactions in environmental remediation processes: uncertainty and challenges, Appl. Catal., B 224 (2018) 973–982.
[52] X. Duan, H. Sun, M. Tade, S. Wang, Metal-free activation of persulfate by cubic mesoporous carbons for catalytic oxidation via radical and nonradical processes, Catal. Today 307 (2018) 140–146.
[53] X. Duan, H. Sun, S. Wang, Metal-free carbocatalysis in advanced oxidation reactions, Acc. Chem. Res. 51 (2018) 678–687.
[54] H. Sun, S. Liu, G. Zhou, H.M. Ang, M.O. Tade, S. Wang, Reduced graphene oxide for catalytic oxidation of aqueous organic pollutants, ACS Appl. Mater. Inter. 4 (2012) 5466–5471.
[55] Z. Pei, L. Li, L. Sun, S. Zhang, X.Q. Shan, S. Yang, B. Wen, Adsorption characteristics of 1,2,4-trichlorobenzene, 2,4,6-trichlorophenol, 2-naphthol and naphthalene on graphene and graphene oxide, Carbon 51 (2013) 156–163.
[56] J. Wang, X. Gao, Y. Wang, C. Gao, Novel graphene oxide sponge synthesized by freeze-drying process for the removal of 2,4,6-trichlorophenol, RSC Adv. 4 (2014) 57476–57482.
[57] C. Liang, H.-W. Su, Identification of sulfate and hydroxyl radicals in thermally activated persulfate, Ind. Eng. Chem. Res. 48 (2009) 5558–5562.
[58] G.V. Buxton, C.L. Greenstock, W.P. Helman, A.B. Ross, Critical Review of rate constants for reactions of hydrated electrons, hydrogen atoms and hydroxyl radicals (·OH/·O− in Aqueous Solution, J. Phys. Chem. Ref. Data 17 (1988) 513–886.
[59] R.E. Huie, C.L. Clifton, Rate constants for hydrogen abstraction reactions of the sulfate radical, SO_4^{-}. Alkanes and ethers, Int. J. Chem. Kinet. 21 (1989) 611–619.
[60] E. Saputra, S. Muhammad, H. Sun, H.-M. Ang, M.O. Tade, S. Wang, Shape-controlled activation of peroxymonosulfate by single crystal alpha-Mn_2O_3 for catalytic phenol degradation in aqueous solution, Appl. Catal., B 154 (2014) 246–251.
[61] E. Saputra, X. Duan, J.A. Pinem, S. Bahri, S. Wang, Shape-controlled Co_3O_4 catalysts for advanced oxidation of phenolic contaminants in aqueous solutions, Sep. Purif. Technol. 186 (2017) 213–217.
[62] X. Liu, G. Liu, L. Wang, Y. Li, Y. Ma, J. Ma, Morphology- and facet-controlled synthesis of CuO micro/nanomaterials and analysis of their lithium ion storage properties, J. Power Sources 312 (2016) 199–206.
[63] J. Liu, X. Huang, Y. Li, K.M. Sulieman, X. He, F. Sun, Self-assembled CuO monocrystalline nanoarchitectures with controlled dimensionality and morphology, Cryst. Growth Des. 6 (2006) 1690–1696.